Quasicubic α-Fe_2O_3 Nanoparticles with Excellent Catalytic Performance

Yuanhui Zheng,[†] Yao Cheng,[†] Yuansheng Wang,*[,†] Feng Bao,[†] Lihua Zhou,[†] Xiaofeng Wei,[‡] Yingying Zhang,[‡] and Qi Zheng[‡]

State Key Laboratory of Structural Chemistry, Fujian Institute of Research on the Structure of Matter, Chinese Academy of Sciences, Graduate School of Chinese Academy of Sciences, Fuzhou, Fujian, 350002, China and National Engineering Research Center of Fertilizer Catalyst, Fuzhou University, Fuzhou, Fujian, 350002, China

Received: November 15, 2005; In Final Form: December 31, 2005

Uniform quasicubic α-Fe_2O_3 nanoparticles enclosed by six identical {110} planes were synthesized by a simple solvothermal method. TEM investigations revealed that they were formed through oriented attachment of primary nanocrystals assisted by Ostwald ripening, and PVP surfactant played an important role in control over the final morphology of the products. These quasicubic nanoparticles could catalyze oxidation of almost 100% CO at a temperature of 230 °C, much lower than those of nanophases with flowerlike, hollow, or other forms of irregular external morphologies having various crystal planes exposed to the gas, indicating that the external morphology and especially the exposure crystal planes of α-Fe_2O_3 nanocatalyst affect the catalytic activity more significantly than the traditionally accepted factors (such as high BET surface area, hollow structure, etc.) do for CO catalytic oxidation.

1. Introduction

Aiming at novel functional materials, much effort has been focused on synthesis of monodispersed nanocrystals with various shapes.[1−4] The interest in this subject is due to the knowledge that the physical and chemical properties of materials depend not only on the chemical composition but crucially also on their size and shape.[5] It is expected that tailoring the size and external morphology of nanocrystals would endow them with unique properties. Thus, a carefully directed improvement of the properties, especially with regard to specific applications, has to be combined with tailor of the materials' chemical, structural, and morphological characteristics. In particular, the required chemical composition, size, and shape of nanocrystals represent the main goals of preparative approaches and can be achieved by appropriate adjustment of all synthesis parameters including solvent, surfactant, temperature/time, pH value, etc.

Recently, environmental problems such as air and water pollution have provided the impetus for sustained fundamental and applied research in the area of environmental remediation. As for the elimination of CO gas, the catalytic oxidation of CO with O_2 attracts much attention. It is known from the literature that there are noble-metal-free[6−8] and noble-metal-containing[9−11] oxide catalysts for CO oxidation. Compared to the former, the latter exhibits superior catalytic properties but is much more expensive. Exploiting low-cost catalysts with excellent performance is an important task in this field. Recently, the catalytic activity of low-cost noble-metal-free oxide catalysts has been enhanced remarkably due to their nanostructures, such as small particle size, high specific surface area,[6] hollow structure,[7] and, if available, regular shape with definite exposure planes.[12,13] However, the exact origin and the determining factors of catalytic activity are still not clear. The aim of this work was to synthesize noble-metal-free oxide nanocatalysts with novel architectures and investigate the main factors affecting their catalytic performance.

Hematite (α-Fe_2O_3), based on hexagonal close packing of oxygen with iron in 2/3 of the octahedral vacancies, is traditionally used as catalysts, pigments, gas sensors, and electrode materials[14−17] due to its low cost, high resistance to corrosion, and environmentally friendly properties. Stimulated by the promising applications of ferric oxides nanomaterials, various nanostructured α-Fe_2O_3 crystals have been synthesized through thermal decomposition, thermal oxidation, and hydrothermal methods.[17−19] Recently, as a new strategy for synthesizing transition-metal oxides, a mediated *N*-dimethylformamide (DMF) solvothermal route has been adopted to prepare hollow Cu_2O nanospheres and α-Fe_2O_3 nanoparticles (with DMF as a reactant).[20,21] Herein, we present its use, for the first time, to synthesize monodispersed single-crystalline quasicubic α-Fe_2O_3 nanoparticles about 40 nm in size using ferric nitrate as the metal-ion source in the presence of poly(*N*-vinyl-2-pyrrolidone) (PVP). The morphologies of such nanoparticles are tunable by adjusting the synthesis parameters. The as-prepared α-Fe_2O_3 nanocatalyst was characterized for catalytic oxidation of carbon monoxide, and the results demonstrated that the quasicubic α-Fe_2O_3 is a much superior catalyst than the other forms of nano- and microsized ferric oxide catalysts in terms of activation temperature, conversion efficiency, and thermal stability in the catalytic reaction.

2. Experimental Section

2.1. Preparation of α-Fe_2O_3 Nanoparticles. Ferric nitrate and *N*,*N*-dimethylformamide (DMF) of analysis grade were purchased from Shanghai Chemical Reagent Ltd., China, and poly(*N*-vinyl-2-pyrrolidone) (PVP, $M_w = 30\,000$) was purchased from Sigma-Aldrich Chemical Co. Monodispersed quasicubic α-Fe_2O_3 nanoparticles were synthesized through a facile solvothermal route in the present of PVP. In a typical experiment,

* Corresponding author. Phone/Fax: +86-591-8370-5402. E-mail: yswang@fjirsm.ac.cn.
[†] Chinese Academy of Sciences.
[‡] Fuzhou University.

10.1021/jp056617q CCC: $33.50
Published on Web 01/31/2006

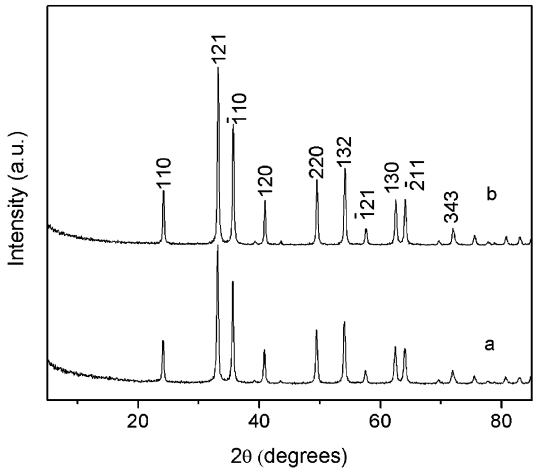

Figure 1. XRD patterns of the as-synthesized samples: (a) flowerlike and (b) quasicubic nanoparticles.

0.404 g of $Fe(NO_3)_3 \cdot 9H_2O$ and 0.600 g of PVP (molar ratio of PVP to iron salt of 2×10^{-2}:1) were dissolved in 36 mL of DMF. The solution was then turned into a Teflon-lined stainless steel autoclave of 70 mL capacity. The sealed tank was put into an oven and heated at 180 °C for 30 h. After reaction, the autoclave was cooled to room temperature naturally. The red precipitates were collected by centrifugation, washed with deionized water and ethanol several times, and finally dried in the air at room temperature. The flowerlike α-Fe_2O_3 nanoparticles were synthesized in the same way without the surfactant (PVP) for 3 h.

2.2. Structural Characterizations. The powder X-ray diffraction (XRD) patterns of the as-prepared samples were recorded by a RIGAKU-DMAX2500 X-ray diffractometer using Cu Kα radiation ($\lambda = 0.154$ nm) at a scanning rate of 5°/min for 2θ ranging from 5° to 85°. To determine the textural properties of the as-prepared samples, nitrogen adsorption−desorption measurements were carried out at 77 K using a Micrometrics ASAP 2020 system after the sample was degassed at 120 °C in a vacuum overnight. The microstructures and morphologies of the samples were investigated by a JEOL-2010 transmission electron microscope (TEM) working at 200 kV and a JSM-6700F scanning electron microscope (FESEM) working at 20 kV. In a brief procedure, samples of nanoparticles were redispersed in ethanol by ultrasonic agitation. A small volume of the suspension was dropped on the carbon-enhanced copper grids and dried in air.

2.3. Catalytic Activity Measurements. Measurements of the catalytic activity for the carbon monoxide oxidation reaction of the above prepared samples were carried out in a quartz flow tube reactor (Supporting Information, SI-1) with a gas mixture typically containing 3.33% CO, 6.67% O_2, and 90% N_2 at 360 mL/min in the temperature range from 150 to 300 °C. The composition of the reactants and product was analyzed by a gas chromatograph (GC-14C) equipped with a thermal conductivity detector (TCD).

3. Results and Discussion

The XRD patterns of the as-synthesized samples with flowerlike and quasicubic morphologies are shown in Figure 1, where all the diffraction peaks are in good agreement with that of the standard pattern for rhombohedral α-Fe_2O_3 (space group: $R\bar{3}c$, with lattice constants $a = b = c = 0.542$ nm and $\alpha = 55.2$ (PDF # 850987)). The textural properties of flowerlike and quasicubic particles (Supporting Information, SI-2) were characterized by Brunauer−Emmett−Teller (BET) gas sorptometry measurements, and the corresponding BET surface area is 39.9 and 18.3 m^2/g, respectively.

TEM and SEM observations revealed the flowerlike and quasicubic morphologies of α-Fe_2O_3 nanoparticles, as shown in Figure 2. In the system without PVP and reacted at 180 °C for 3 h, a high yield of three-dimensional flowerlike α-Fe_2O_3 single crystals sized 30−50 nm was formed (Figure 2a). The magnified TEM image of an individual particle (inset in Figure 2a) indicated the flowerlike morphology. When the reaction time was prolonged to 30 h, the flowerlike α-Fe_2O_3, formed as a result of oriented attachment of several smaller nanocrystals, then evolved to the hexahedral nanoparticles through Ostwald ripening, as already described in our previous paper.[21] However, when the system was added with PVP and reacted for 30 h, regular nanoparticles with a smooth surface and a narrow size distribution from 30 to 50 nm were obtained, as shown in Figure 2b. The high-magnification SEM image (inset in Figure 2b) of a single particle revealed their regular quasicubic morphology (more SEM/TEM images are given in Supporting Information SI-3). A typical high-resolution TEM (HRTEM) image of a single quasicubic α-Fe_2O_3 nanocrystal (Figure 2c) shows the uniform lattice structure, free of detectable defects. Its corresponding fast Fourier transform (FFT) pattern (inset in Figure 2c) is indexed to a trigonal α-Fe_2O_3 crystal along the $[1\bar{1}1]$ zone axis, indicating that the four side facets of the crystal are {110} planes. On the basis of the fact that FFT patterns from the HRTEM images of all the individual α-Fe_2O_3 nanocrystals exhibit the same reciprocal plane, we presented a structural model of a quasicubic hexahedron enclosed by six identical facets of {110} planes, as shown in Figure 2d, for these α-Fe_2O_3 nanocrystals.

To reveal the growth mechanism of the quasicubic α-Fe_2O_3 nanoparticles in more detail, the products were collected at certain reaction time intervals for TEM observations. Figure 3 shows the representative TEM images of the products prepared at 180 °C for 3, 10, 20, and 30 h. At the early reaction stage (reacted for 3 h), α-Fe_2O_3 primary nanocrystals about 5 nm in size were formed, as shown in Figure 3a. When the reaction time was prolonged to 10 h, driven by the minimization of surface energy, many neighboring primary nanocrystals aggregated together through oriented attachment to form three-dimensional flowerlike particles sized 40−50 nm, as demonstrated in Figure 3b. The upper inset of Figure 3b is the HRTEM image of an individual flowerlike particle (the area in the square is magnified and presented in Supporting Information SI-4, showing the lattice structure more clearly), and the corresponding FFT pattern (the lower inset of Figure 3b) demonstrates its monocrystalline nature. After the reaction was further prolonged to 20 h, instead of the flowerlike nanoparticles, the quasicubic ones appeared, as presented in Figure 3c. In the HRTEM image of a quasicubic crystal shown in the inset of Figure 3c, several primary nanocrystals (highlighted by circles) are found glued coherently to the particle at the corners due to oriented attachment (the magnified image is presented in Supporting Information SI-4). It is notable that, besides the flowerlike and quasicubic α-Fe_2O_3 nanoparticles, some small primary nanocrystals still existed in the samples synthesized for 10 and 20 h, indicating that oriented attachment is still underway. However, after reacting for 30 h, there were only monodispersed quasicubic α-Fe_2O_3 particles with smooth surfaces in this sample, as shown in Figure 3d.

It has been found in our previous study that the primary α-Fe_2O_3 nanocrystals were capped with DMF molecules acting

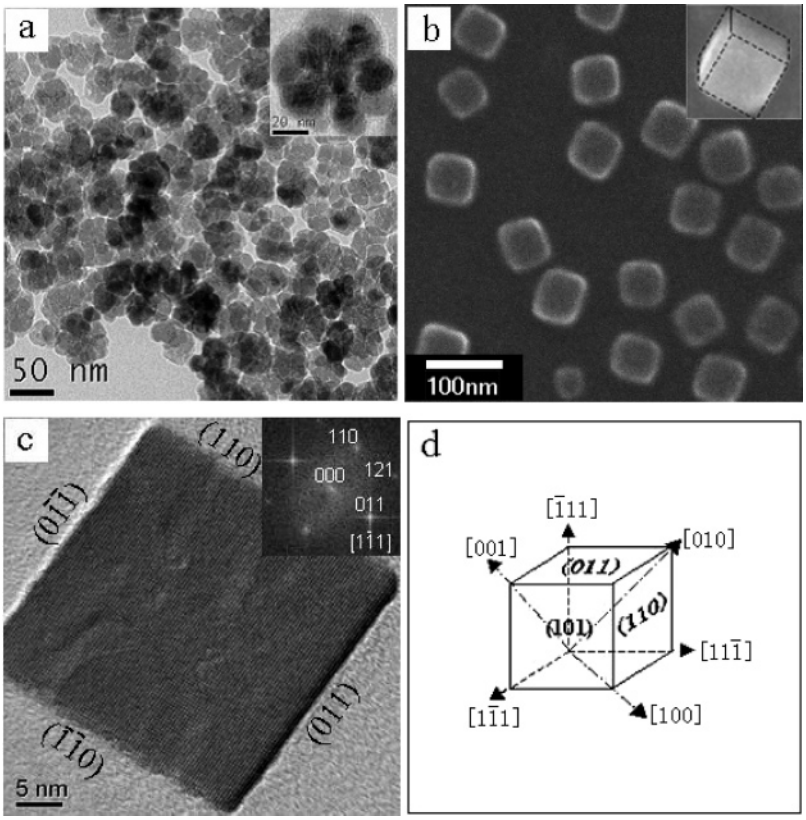

Figure 2. (a) TEM image of flowerlike α-Fe_2O_3 nanoparticles, (b) SEM image of quasicubic α-Fe_2O_3 nanoparticles, (c) HRTEM image of a single quasicubic α-Fe_2O_3 nanoparticle and its FFT pattern, and (d) structural model of the quasicubic α-Fe_2O_3 nanoparticle; the insets in Figure 2a and 2b are magnified TEM and SEM images of an individual flowerlike and quasicubic α-Fe_2O_3 nanoparticle, respectively.

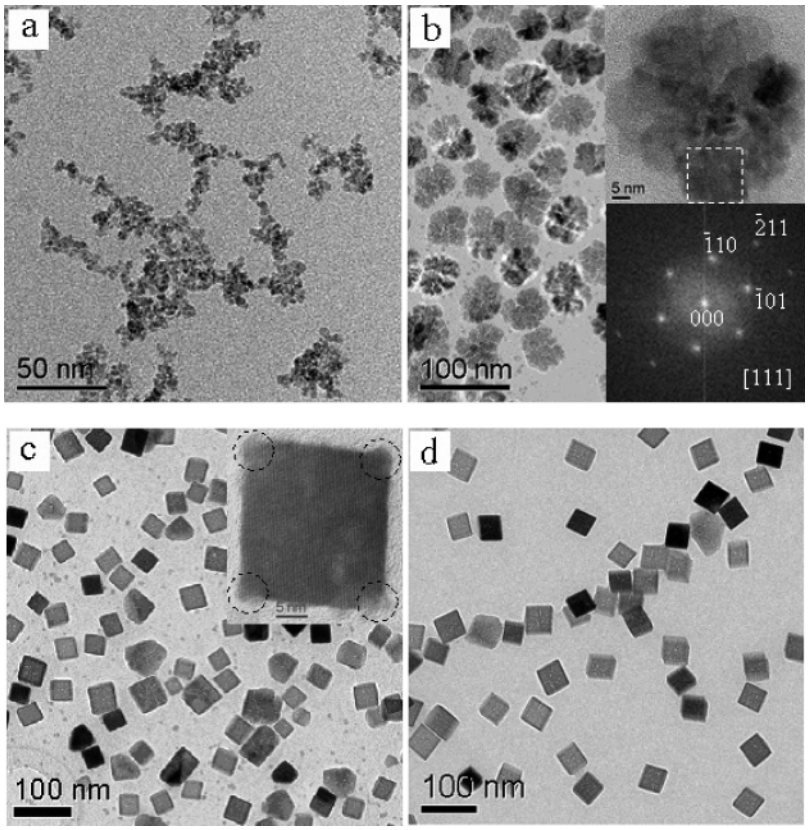

Figure 3. TEM micrographs of the samples prepared at 180 °C for different reaction periods: (a) 3, (b) 10, (c) 20, and (d) 30 h, respectively.

as ligands.[21] The amount of DMF adsorbed on different surface planes depends on the density of the iron atom on the corresponding planes, and the higher the density, the more DMF will be adsorbed. It was calculated that the density of the iron atom on the low-index crystal planes of {110}, {111}, and {100} of α-Fe_2O_3 is 10.1, 7.9, and 4.1 atoms/nm^2, respectively.

The {110} planes with a relatively higher density of iron atom adsorb more DMF molecules; thus, they would grow slower during the oriented attachment of primary nanocrystals than the other planes, as described by Zhang et al. for the CuO system,[22] tending to form nanoparticles enclosed by {110} exposure planes. In addition, to study the role of PVP in determining the final shape of as-obtained nanoparticles, the relationship between the ratio of PVP to iron salt and the parameters (size, shape) of α-Fe_2O_3 nanoparticles was examined (TEM images of α-Fe_2O_3 nanoparticles synthesized under various molar ratios of PVP to iron salt are shown in Supporting Information SI-5). It was found that PVP surfactant contributed not only to stabilizing and dispersing the α-Fe_2O_3 nanoparticles, but also to controlling the formation of the quasicubic geometry. If there was no PVP in the reaction solution, most of the nanoparticles were truncated or uncompleted quasicubes. As PVP was added and the amount was increased, the primary nanoparticles capped with long carbon chains of PVP had longer to select their right positions during the course of oriented attachment due to the slower aggregation rate, thus favoring formation of the final regular quasicubic morphology. However, the particle size stayed basically the same for the samples with different ratios of PVP to iron salt, implying that it was not remarkably affected by PVP.

Carbon monoxide catalytic oxidation is an important process in three-way catalysis. The traditional micrometer α-Fe_2O_3 catalyst has low catalytic activity for oxidization of carbon monoxide. Li et al. reported that α-Fe_2O_3 nanocatalyst with a diameter of ca. 3 nm and large BET surface area of 250 m^2/g could catalyze the oxidization of almost 100% carbon monoxide at temperatures above 350 °C, obviously better than that of traditional micrometer α-Fe_2O_3 catalyst, and they ascribed the improvement of catalytic activity to the much higher specific surface area of the nanoparticles.[6] Besides, the hollow α-Fe_2O_3 nanowires with an average outer diameter and length of ca. 50 nm and 1−2 μm, respectively, further promoted the catalytic activity by decreasing the lowest complete conversion temperature (denoted by $T_{100\%}$) to 320 °C, which is regarded to originate from the hollow structure of the material.[7] It is generally accepted that the catalytic process is mainly related to the adsorption and desorption of gas molecules on the surface of the catalyst. The high specific surface area of the nanocatalysts results in more unsaturated surface coordination sites exposed to the gas. In addition, the interconnected hollow pores in the catalyst enable storage of more gas molecules. Therefore, the enhancement of catalytic activity by high specific surface area and hollow structure is reasonable.

The catalytic effectiveness over flowerlike and quasicubic α-Fe_2O_3 nanoparticles in our experiments is revealed in Figure 4. A 100 mg amount of quasicubic α-Fe_2O_3 nanoparticles can catalyze oxidation of 100% CO to CO_2 at a temperature as low as 230 °C in an inlet gas mixture of 3.33% CO and 6.67% O_2 at 360 mL/min for the first run, while the same amount of flowerlike α-Fe_2O_3 nanoparticles can only catalyze oxidation of less than 5% CO to CO_2 under identical conditions. The $T_{100\%}$ of flowerlike nanoparticles was about 30 °C higher than that of quasicubic nanoparticles. It is also noteworthy that both α-Fe_2O_3 catalysts with different morphologies were activated in a very narrow temperature range (less than 5 °C), much smaller than that previously reported for other α-Fe_2O_3 nanocatalysts,[6,7] which should be ascribed to their prominent size and shape homogeneity. This unusual characteristic would find an important application in CO gas sensors. To test the thermal stability of quasicubic α-Fe_2O_3 catalyst, two additional runs were performed after the reactor was completely cooled to ambient temperature. The experimental data are shown in Figure 5. The $T_{100\%}$ for the second and third runs increased only 5 and 15 °C from that for the first one, respectively, revealing the excellent thermal stability and recycling performance of the quasicubic α-Fe_2O_3 catalyst (as a comparison, the $T_{100\%}$ upward shifts for the second and third runs were 50 and 60 °C in Li's work[6] and 12 and 28 °C in Xiong's work,[7] respectively). The upward shifting of the $T_{100\%}$ is thought to relate to the agglomeration of α-Fe_2O_3 nanoparticles and the change of their shape during the measurements (Supporting Information SI-6).

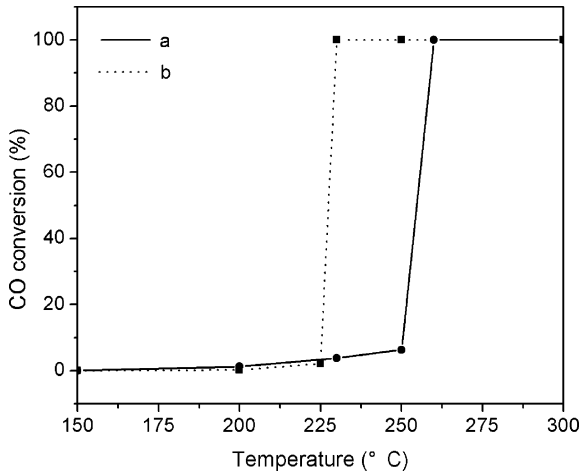

Figure 4. Comparison of the carbon monoxide conversion efficiencies between (a) flowerlike and (b) quasicubic α-Fe_2O_3 nanoparticles.

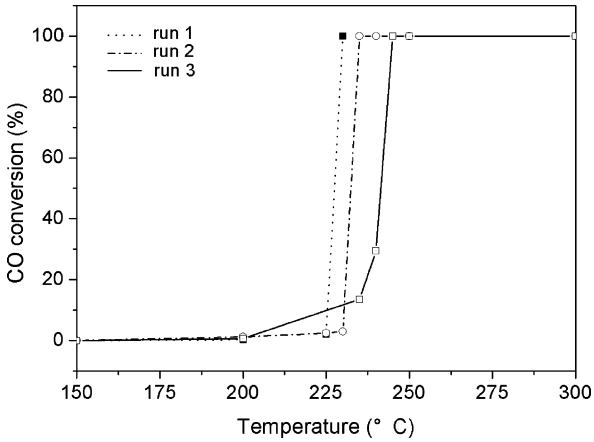

Figure 5. Percentage conversion versus temperature curves for the catalytic oxidation of CO over quasicubic α-Fe_2O_3 nanoparticles for three runs.

It is surprising that, despite the smaller BET surface area and pore-free structure, the catalytic performance of quasicubic α-Fe_2O_3 nanoparticles is remarkably better than that of the other forms of α-Fe_2O_3 nanomaterials mentioned above. Naturally a question comes to mind: what caused the excellent catalytic performance of the quasicubic α-Fe_2O_3 catalyst? It may be helpful to recall the specific morphologies of these ferric oxide nanomaterials. As described above, the uniform quasicubic α-Fe_2O_3 nanoparticles are all enclosed by six equivalent {110} planes, which may be exactly the answer to the question. It was reported that, for CO catalytic oxidation over Fe_2O_3, CO adsorbs on a surface Fe site first and is then oxidized by the surrounding less coordinated O atom; subsequent attachment of CO and O_2 to Fe sites results in the formation of a CO_3 complex, and the formation heat is enough to allow CO_2 to leave the surface, reverting the system to Fe_2O_3.[23] Therefore, Fe sites

on the surfaces should act as the active species for the catalytic reaction. Thus, we conclude that the high density of Fe atoms on the exposure {110} planes leads to the predominance in catalytic performance of quasicubic α-Fe_2O_3 nanocrystals over that of the nanophase with flowerlike, hollow, or other forms of irregular external morphologies having various crystal planes exposed to the gas.

4. Conclusion

We successfully synthesized monodispersed quasicubic α-Fe_2O_3 nanoparticles with excellent catalytic performance for CO oxidation through a simple solvothermal method. Their shape is largely controlled by the experimental parameters, such as reaction duration and surfactant. It is evident that the nanostructures of catalysts are very important to their catalytic performance, and the specific exposure crystal planes with relative higher density of active species (e.g., {110}) affect the catalytic performance more significantly than the traditionally accepted factors (such as high BET surface area, hollow structure, etc.) do for CO catalytic oxidation. The enhancement of catalytic performance for CO oxidation, especially the remarkable decreasing of the lowest complete conversion temperature ($T_{100\%}$), may promote the application of α-Fe_2O_3 nanocatalyst in many fields, such as gas purification (e.g., automobile tail gas elimination and cigarette filtering) and carbon monoxide gas sensors.

Acknowledgment. This work was supported by the project of Nano-molecular Functional Materials of Fujian Province (2005HZ01-1), a grant from the Natural Science Foundation of Fujian Province (A0320001), and the State Key Laboratory of Structural Chemistry of China (050005).

Supporting Information Available: Schematic diagram of the flow tube reactor setup for catalytic activity measurement, more SEM and TEM images. and the textural properties of the products. This material is available free of charge via the Internet at http://pubs.acs.org.

References and Notes

(1) Zeng, H.; Rice, P. M.; Wang, S. X.; Sun, S. *J. Am. Chem. Soc.* **2004**, *126*, 11458.

(2) Si, R.; Zhang, Y.; You, L.; Yan, C. *Angew. Chem., Int. Ed.* **2005**, *21*, 3256.

(3) Yang, H. G.; Zeng, H. C. *Angew. Chem., Int. Ed.* **2004**, *44*, 5930.

(4) Sun, Y.; Mayers, B.; Herricks, T.; Xia, Y. *Nano Lett.* **2003**, *3*, 955.

(5) Suryanarayana, C.; Koch, C. C. *Non-Equilibrium Processing of Materials;* Pergamon Materials Series; Pergamon Press: New York, 1999.

(6) Li, P.; Miser, D. E.; Rabiei, S.; Yadav, R. T.; Hajaligol, M. R. *Appl. Catal. B: Environ.* **2003**, *43*, 151.

(7) Xiong, Y.; Li, Z.; Li, X.; Hu, B.; Xie, Y. *Inorg. Chem.* **2004**, *43*, 6540.

(8) Zhou, K.; Wang, X.; Sun, X.; Peng, Q.; Li, Y. *J. Catal.* **2005**, *229*, 206.

(9) Zhang, X.; Wang, H.; Xu, B. Q. *J. Phys. Chem. B* **2005**, *109*, 9678.

(10) Glaspell, G.; Fuoco, L.; El-Shall, M. S. *J. Phys. Chem. B* **2005**, *109*, 17350.

(11) Yang, J. H.; Henao, J. D.; Raphulu, M. C.; Wang, Y.; Caputo, T.; Groszek, A. J.; Kung, M. C.; Scurrell, M. S.; Miller, J. T.; Kung, H. H. *J. Phys. Chem. B* **2005**, *109*, 10319.

(12) Ohko, Y.; Ando, I.; Niwa, C.; Tatsuma, T.; Yamamura, T.; Nakashima, T.; Kubota, Y.; Fujishima, A. *Environ. Sci. Technol.* **2001**, *35*, 2365.

(13) Choudary, B. M.; Mulukutla, R. S.; Klabunde, K. J. *J. Am. Chem. Soc.* **2003**, *125*, 2020.

(14) Faust, B. C.; Hoffmann, M. R.; Bahnemann, D. W. *J. Phys. Chem.* **1989**, *93*, 6371.

(15) Cornell, R. M.; Schwertmann, U. *The Iron Oxides. Structure, Properties, Reactions, Occurrence and Uses*; VCH: Weinheim, 1996; p 464.

(16) Han, J. S.; Bredow, T.; Davey, D. E.; Yu, A. B.; Mulcahy, D. E. *Sens. Actuators, B* **2001**, *75*, 18.

(17) Chen, J.; Xu, L.; Li, W.; Gou, X. *Adv. Mater.* **2005**, *17*, 582.

(18) Wen, X.; Wang, S.; Ding, Y.; Wang, Z. L.; Yang, S. *J. Phys. Chem. B* **2005**, *109*, 215.

(19) Niederberger, M.; Krumeich, F.; Hegetschweiler, K.; Nesper, R. *Chem. Mater.* **2002**, *14*, 78.

(20) Chang, Y.; Teo, J. J.; Zeng, H. C. *Langmuir* **2005**, *21*, 1074.

(21) Zheng, Y.; Cheng, Y.; Wang, Y.; Bao, F. *J. Cryst. Growth* **2005**, *284*, 221.

(22) Zhang, Z.; Sun, H.; Shao, X.; Li, D.; Yu, H.; Han, M. *Adv. Mater.* **2005**, *17*, 42.

(23) Reddy, B. V.; Rasouli, F.; Hajaligol, M. R.; Khanna, S. N. (a) *Fuel* **2004**, *83*, 1537. (b) *Chem. Phys. Lett.* **2004**, *384*, 242.